

Optimization of the luminescence emission in nanocrystalline SiGe/SiO₂ multilayers

A. Rodríguez^{*,1}, M. I. Ortiz², J. Sangrador¹, T. Rodríguez¹, M. Avella³, A. C. Prieto³, J. Jiménez³, A. Kling^{4,5}, and C. Ballesteros²

¹ Dpto. Tecnología Electrónica, E.T.S.I.T., Universidad Politécnica de Madrid, 28040 Madrid, Spain

² Dpto. Física, E.P.S., Universidad Carlos III de Madrid, 28911 Leganés (Madrid), Spain

³ Dpto. Física de la Materia Condensada, Universidad de Valladolid, 47011 Valladolid, Spain

⁴ Instituto Tecnológico e Nuclear, Estrada Nacional 10, 2686-953 Sacavém, Portugal

⁵ Centro de Física Nuclear da Universidade de Lisboa, 1649-003 Lisbon, Portugal

Received 16 October 2006, revised 15 February 2007, accepted 15 February 2007

Published online 16 May 2007

PACS 68.37.Lp, 68.65.Ac, 78.60.Hk, 81.07.Bc, 81.15.Gh, 82.80.Yc

Luminescent multilayers of SiGe nanocrystals embedded in an oxide matrix have been fabricated by Low Pressure Chemical Vapour Deposition of SiGe and SiO₂ in a single run followed by a Rapid Thermal Annealing treatment to crystallize the SiGe nanoparticles. Structural parameters like the diameter of the nanoparticles and the oxide interlayer thickness, as well as the annealing conditions have been investigated in order to get the maximum intensity of the luminescence emission. Structures with small nanoparticles (3–4.5 nm) separated by thick oxide barriers (≈35 nm) annealed at 900 °C for 60 s yield the maximum intensity as a result of a compromise between the appropriate crystallization of the small nanoparticles and a reduced degradation of their composition by Ge diffusion. An additional treatment at 450 °C in forming gas for dangling-bond passivation increases the intensity of the luminescence by 25%.

© 2007 WILEY-VCH Verlag GmbH & Co. KGaA, Weinheim

1 Introduction

Group IV (Si or Ge) nanocrystals embedded in SiO₂ have applications in non volatile memories and optoelectronic devices fully compatible with the CMOS technology [1–4]. The diameter of the nanoparticles should be adapted to the specific application, but for all of them it must be uniform and of a few nanometers. Also, the spatial distribution must be uniform with a nanoparticle areal density above $5 \times 10^{11} \text{ cm}^{-2}$. SiGe nanocrystals with controlled composition and size and the appropriate areal density embedded in an oxide matrix have been obtained by Low Pressure Chemical Vapour Deposition (LPCVD) of amorphous discontinuous SiGe films followed by an annealing process to crystallize the nanoparticles [5]. Luminescence emission with a main band peaking at a wavelength of 400 nm was detected previously in this kind of structures, but its intensity was not optimized [6]. In this work, the structural features of the samples, i.e. the diameter of the nanoparticles and the thickness of the SiO₂ inter-dielectric layers (IDL), the post-growth annealing processes for nanoparticle crystallization and the effect of additional thermal treatments in an atmosphere containing H₂ have been investigated with the aim of the maximization of the luminescence intensity.

* Corresponding author: e-mail: andres.rodriguez.dominguez@upm.es

2 Experimental procedures

2.1 Samples preparation

Multilayer structures with five periods of amorphous SiGe nanoparticles/SiO₂ and a top SiO₂ capping layer were deposited to increase the areal density of nanoparticles. The deposition processes were carried out in a Tempress commercial LPCVD reactor operating at a low constant temperature of 390 °C and a total pressure of 50 mTorr according to the procedures described elsewhere [5]. The SiGe nanoparticles, with a Ge fraction of $x \approx 0.4$, were deposited using Si₂H₆ and GeH₄ with a gas flow ratio of GeH₄/Si₂H₆ = 0.82. The SiO₂ layers were deposited using Si₂H₆ and O₂ with a flow ratio of Si₂H₆/O₂ = 0.2. Four types of samples were fabricated, as summarized in Table 1. The SiGe deposition time was 60 min for samples A and B and 25 min for samples C and D, yielding nanoparticles of two different diameters (d). IDL of three different thicknesses (t) were deposited by varying the SiO₂ deposition time.

The crystallization of the nanoparticles was achieved by subsequent annealing of the samples in N₂ atmosphere at temperatures between 700 and 1000 °C for times up to 120 s using a Jipelec FAV4 Rapid Thermal Annealing (RTA) unit. Selected samples were further annealed in an open tube furnace at 450 °C for 30 min exposed to a high flow of forming gas (10% H₂ + 90% N₂). Pure SiO₂ films were also deposited and annealed in the same conditions than the SiGe/SiO₂ multilayers for comparison.

2.2 Characterization techniques

Transmission Electron Microscopy (TEM) with high resolution (HREM) was used to study the shape of the nanoparticles, to determine their size, distribution and areal density and to estimate, when possible, their composition. The crystallization of the nanoparticles in the annealed samples was also studied. Cross-sectional specimens were prepared by mechanical grinding, dimpling and argon ion-milling of the samples in a liquid-nitrogen-cooled holder with an acceleration voltage of 3 kV and an incidence angle of 8°. The studies were carried out using a Philips Tecnai 20F FEG microscope operating at 200 kV, equipped with an Energy Dispersive X-Ray (EDX) analysis system. Fourier transform patterns (FFT) of the HREM images and subsequent filtering were used to improve the contrast and verify the nanoparticle crystallization. Raman spectroscopy was used to analyze the crystallization of the nanoparticles. The spectra were acquired using a Jobin Yvon HR Labram spectrometer operating in backscattering geometry. The excitation was done with the 325 nm line of an He–Cd laser and the detection was performed with a liquid nitrogen cooled CCD multichannel detector. The Raman spectra of amorphous and crystalline SiGe alloys are described in the Ref. [7]. Rutherford Backscattering Spectrometry (RBS) was used to study the effect of the thermal treatments on the structure of the samples. The experimental measurements were performed using a 2 MeV 4He⁺ beam. A tilt angle of 78° in Cornell geometry was chosen in order to increase the depth resolution. The detector was located at 160° with respect to the incident beam. The spectra were interpreted using the RUMP simulation code [8] combined with the modelling methods described elsewhere [9]. The cathodoluminescence (CL) emission of the samples was measured in a XiCLOne system (Gatan) attached to a SEM (JEOL 820). The spectra were measured at liquid nitrogen temperature using an e-beam acceleration voltage of 5 kV and a beam current of 10 nA.

Table 1 Structural features of the four samples fabricated.

sample	diameter of the SiGe nanoparticles d (nm)	thickness of the SiO ₂ IDL t (nm)
A	≥ 5	5
B	≥ 5	35
C	3–4.5	15
D	3–4.5	35

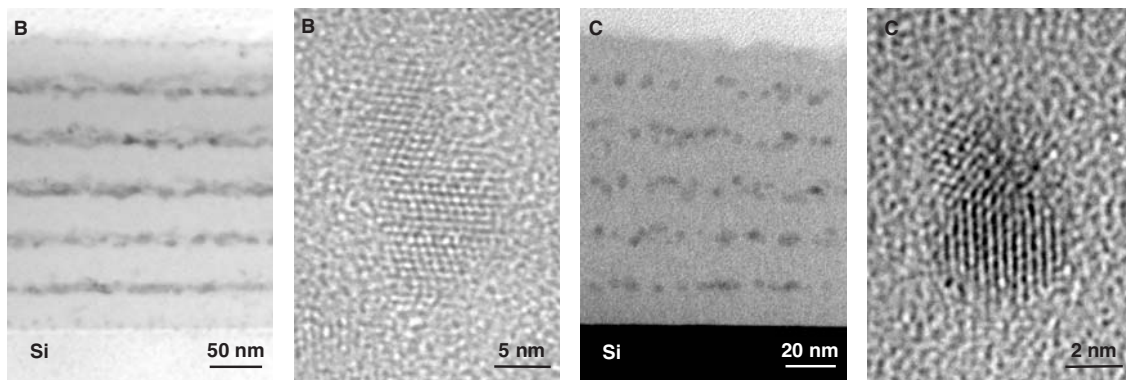


Fig. 1 Cross-sectional TEM images of samples B (large nanoparticles and thick oxide interlayers) and C (small nanoparticles and thin oxide interlayers) annealed by RTA at 900 °C for 60 s showing the SiGe (dark)/SiO₂ (bright) multilayers. The SiGe nanocrystals are visible in the high resolution filtered images. The Si-substrate was oriented parallel to the $\langle 110 \rangle$ direction for accurate thickness measurements.

3 Results and discussion

3.1 Transmission electron microscopy

Figure 1 shows cross-section TEM and HREM images of samples B and C after annealing at 900 °C for 60 s. The morphology of samples B, C and D (not shown here) after annealing remains unaltered compared to the as-deposited ones (not shown), preserving the nanoparticle density and size after their crystallization. The nanocrystals have diamond structure and contain stacking faults and defects. The average areal density of the nanoparticles could not be estimated in samples A and B because the nanoparticles appear superimposed to each others in the images, and its value is in the interval from $1.2 \times 10^{12} \text{ cm}^{-2}$ to $2.8 \times 10^{12} \text{ cm}^{-2}$ in each layer for samples C and D.

In sample B, stacks of five SiGe layers separated by $\approx 35 \text{ nm}$ thick SiO₂ interlayers are observed in the low magnification images. Due to the two-dimensional projection of the three-dimensional sample, the layers appear to be continuous and their thickness increase from layer to layer. However, higher magnification studies carried out in very thin areas indicate that the layers are discontinuous, and that the increase in the layer thickness is due to an increasing roughness of the layers. EDX spectra obtained in very thin areas of the as-deposited samples indicate that the atomic Ge fraction of the nanoparticles is consistent with the expected value $x \approx 0.4$.

For sample C, stacks of five layers of quasi-spherical SiGe nanoparticles separated by $\approx 15 \text{ nm}$ thick SiO₂ interlayers are observed. In the two layers located at the bottom part of the structure, the nanocrystals follow quasi-straight lines parallel to the Si-substrate, while for the last two layers a higher roughness was observed. EDX spectra acquired in the as-deposited sample show that the nanoparticles, deposited with the same flow ratio used in samples A and B, contain Ge, but in this case their Ge fraction could not be accurately determined from the measurements due to their small size. FFT images show that the lattice parameter of the nanocrystals is intermediate between those of Si and Ge but, with the resolution achieved, it was not possible to accurately determine the Ge content using this procedure.

3.2 Raman spectroscopy

Figure 2 shows Raman spectra of samples A and C (samples with different nanoparticle sizes) after different annealing processes, showing the bands related with Ge–Ge ($275\text{--}300 \text{ cm}^{-1}$), Si–Ge ($375\text{--}400 \text{ cm}^{-1}$) and Si–Si ($\approx 475 \text{ cm}^{-1}$) TO zone edge phonons and the band of crystalline Si (520.2 cm^{-1}) arising from the substrate. In sample A, with large nanoparticles (and also in B, not shown) one observes the Raman signature of crystallized SiGe after annealing at a temperature as low as 700 °C. For increas-

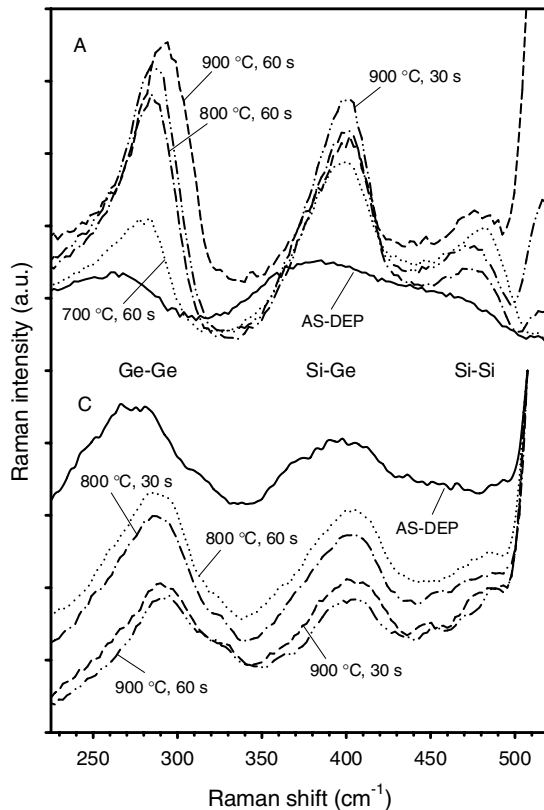


Fig. 2 Raman spectra of samples A (large nanoparticles) and C (small nanoparticles), in both cases with thin oxide interlayers.

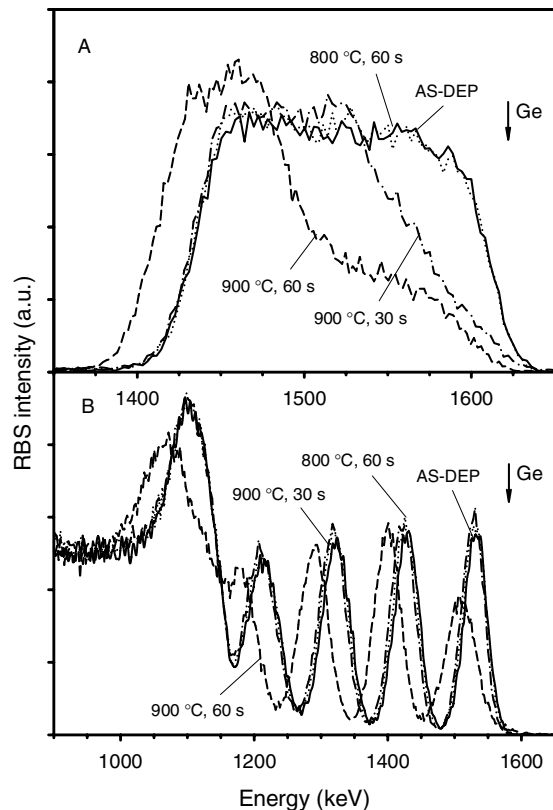


Fig. 3 Ge signal of the RBS spectra of samples A (thin oxide interlayers) and B (thick oxide interlayers), in both cases with large particles.

ing annealing temperature and time, the three characteristic Raman bands are narrowed, their intensities increase and their positions are shifted, which obeys the progressive crystallization of the nanoparticles. Stresses could also contribute to shift the Raman bands, but it is difficult to separate the different contributions. No further improvement of the crystallization is detected after annealing at 900 °C for times above 60 s. The intensity of the Ge–Ge band, relative to that of the other two bands, decreases for high temperature and long time annealing processes, which reveals a reduction of the Ge fraction of the nanocrystals. The Raman signature of SiGe disappears for an annealing temperature of 1000 °C.

In sample C, with small nanoparticle size (and also in D, not shown), one observes the crystallization at temperatures of 800 °C or higher, in agreement with the crystallization data reported for pure Ge nanocrystals of a size equivalent to that of our nanoparticles [10, 11]. No further crystallization is detected if the annealing is prolonged at a fixed temperature. To detect any progress in the crystallization of the nanoparticles, the annealing temperature needs to be increased, being also 900 °C the maximum temperature among those considered in this work at which the Raman bands are still present in the spectra after annealing. The Raman bands of these samples are broader than those observed for samples A and B. This result is due to the phonon confinement, which is significant for particle sizes smaller than 5 nm.

3.3 Rutherford backscattering spectrometry

Figure 3 shows RBS spectra of samples A and B (samples with large particles and different IDL thickness). Due to the different oxide thickness, in samples B, C and D the signals of the individual SiGe

layers are well-separated in the spectra, while in sample A these signals are not resolved. Nevertheless, a reliable analysis of the RBS results is possible in all cases. Simulations of the spectra indicate that the SiGe layers are discontinuous and are best described by a mixture of SiO₂ and SiGe with a Ge fraction of $x = 0.4$. The thickness of the oxide layers have been determined to be in good agreement with those obtained by TEM and with the nominal ones indicated in Table 1. Annealing at temperatures of 800 °C or lower don't cause diffusion of Ge in any of the cases. For sample A, that has the thinnest IDL (≈ 5 nm), annealing at 900 °C causes Ge diffusion, leaving the top layers with a strongly reduced Ge content and destroying the alternated structure. This result is consistent with the reported diffusion length for Ge in SiO₂, which is around 4 nm for an annealing time of 60 s at this temperature [12]. Sample B, with ≈ 35 nm thick SiO₂ interlayers (and also sample D, not shown here), exhibits detectable Ge diffusion only after annealing at 900 °C for 60 s, but the degradation of the structure is mainly restricted to the two SiGe layers located at the top and bottom parts of the multilayer. Annealing at temperatures higher than 900 °C causes the loss of integrity of the structure in all cases.

3.4 Cathodoluminescence

Figure 4 shows the CL spectra of sample D as-deposited and after different annealing treatments as well as the spectra of a pure oxide layer annealed at 900 °C during 60 s. The main spectral feature of the annealed samples is the band peaking at around 400 nm, which is observed for the four samples with SiGe nanocrystals, while it is fully absent in both the as-deposited sample and the annealed oxide layer. Therefore, this band appears clearly correlated to the presence of the SiGe nanocrystals inside the oxide matrix. The intensity of the band depends on the characteristics of the samples, which are related to their structure (nanocrystal size and IDL thickness) and the thermal treatments.

Figure 5 shows the evolution of the intensity of the violet luminescence in the four samples with the annealing conditions. One observes that the luminescence intensity is higher for smaller particle sizes; also, it increases for thicker oxide layers, and finally it increases with the annealing temperature and time. The additional thermal treatment in forming gas at 450 °C causes the intensity of the luminescence to increase by 25%. The effect of this treatment in an atmosphere containing H₂ is the passivation of possible dangling bonds existing in the nanocrystals, thus reducing the amount of non-radiative recombination centers [13].

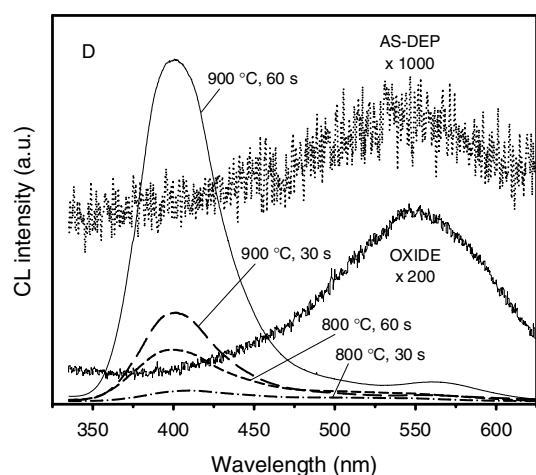


Fig. 4 Luminescence spectra of sample D (small particles and thick oxide interlayers) annealed in different conditions. Spectrum of the annealed oxide.

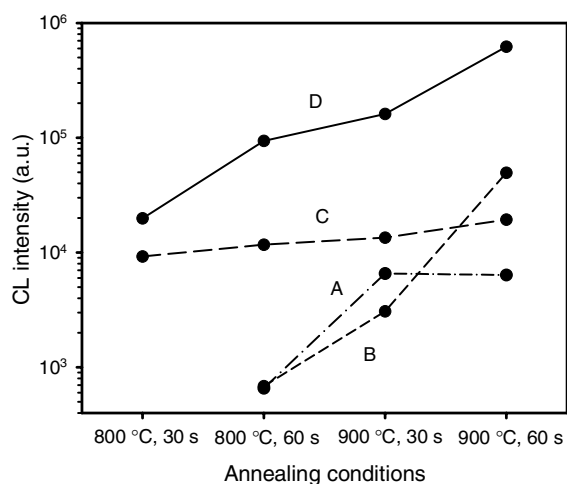


Fig. 5 Intensity of the luminescence emission at 400 nm measured in samples A, B, C and D (see Table 1) annealed in different conditions.

The main luminescence band at 400 nm was also observed in samples with pure Ge nanocrystals embedded in an oxide matrix [14]. Its presence in the spectrum was related to Ge oxygen deficient centers (GeODC) formed at the interface of the nanocrystals with the oxide matrix. The intensity of the luminescence emission is primarily related to the total interface area, which should depend on the areal density of nanocrystals and on their diameter. The luminescence peak energy does not shift for the different samples, ruling out any quantum confinement effect in the mechanism responsible for the luminescence emission. Since the Ge diffusion seems to be more important in samples A and C, with thin IDL, one can argue that the reduction of the Ge fraction of the nanocrystals should lead to a concomitant reduction of the GeODC centers at the interfaces. Nevertheless, further work is necessary to understand the mechanism driving the formation of the GeODC centers during the annealing processes.

4 Summary

Luminescence peaking at 400 nm can be obtained from multilayer structures with SiGe nanocrystals embedded in a SiO₂ matrix. The highest intensity of this emission is obtained in samples with small SiGe nanocrystals (3–4.5 nm) separated by thick oxide barriers (≈ 35 nm), annealed at 900 °C for 60 s. These conditions represent the best compromise that we have found between the appropriate crystallization of the small nanoparticles and their reduced compositional degradation by Ge diffusion, due to the thick SiO₂ interlayers that act as a barrier to such diffusion. The intensity of the luminescence is increased by 25% after a subsequent annealing of the samples at 450 °C in forming gas. The origin of the emission is attributed to Ge oxygen deficient centers formed at the interface between the nanocrystals and the surrounding oxide matrix.

Acknowledgements This work was funded by the Spanish Government through CICYT Project MAT2004-04580-C02-01 and a common grant by CRUP (Portugal) and MCT (Spain) in the framework of the Açções Integradas/Acciones Integradas Program. TEM work has been carried out at the LABMET of the CAM (Madrid).

References

- [1] M. Zacharias, L. X. Yi, J. Heitmann, R. Scholz, M. Reiche, and U. Gösele, *Solid State Phenom.* **94**, 131 (2003).
- [2] T. Z. Lu, M. Alexe, R. Scholz, V. Telelaev, and M. Zacharias, *Appl. Phys. Lett.* **87**, 202110 (2005).
- [3] S. N. M. Mestanza, E. Rodríguez, and N. C. Frateschi, *Nanotechnology* **17**, 4548 (2006).
- [4] T. Stoica and E. Sutter, *Nanotechnology* **17**, 4912 (2006).
- [5] M. I. Ortiz, J. Sangrador, A. Rodríguez, T. Rodríguez, A. Kling, N. Franco, N. P. Barradas, and C. Ballesteros, *phys. stat. sol. (a)* **203**, 1284 (2006).
- [6] M. I. Ortiz, A. Rodríguez, J. Sangrador, T. Rodríguez, M. Avella, J. Jiménez, and C. Ballesteros, *Nanotechnology* **16**, S197 (2005).
- [7] J. Olivares, P. Martín, A. Rodríguez, J. Sangrador, J. Jiménez, and T. Rodríguez, *Thin Solid Films* **358**, 56–61 (2000).
- [8] L. R. Doolittle, *Nucl. Instrum. Methods Phys. Res. B* **9**, 344 (1985); <http://www.genplot.com>.
- [9] A. Kling, M. I. Ortiz, J. Sangrador, A. Rodríguez, T. Rodríguez, C. Ballesteros, and J. C. Soares, *Nucl. Instrum. Methods Phys. Res. B* **249**, 451 (2006).
- [10] G. V. M. Williams, A. Bittar, and H. J. Trodahl, *J. Appl. Phys.* **67**, 1874 (1990).
- [11] M. Zacharias and P. Streintenberger, *Phys. Rev. B* **62**, 8391 (2000).
- [12] K. Shiraishi, Y. Airawa, and S. Kawakami, *J. Lightwave Technol.* **8**, 1151 (1990).
- [13] D. Comedi, O. H. Y. Zalloum, and P. Mascher, *Appl. Phys. Lett.* **87**, 213110 (2005).
- [14] M. Avella, A. C. Prieto, J. Jiménez, A. Rodríguez, J. Sangrador, and T. Rodríguez, *Solid State Commun.* **136**, 224 (2005).